The Spatially-Resolved Star Formation History of the M31 Outer Disc[*]

Edouard J. Bernard,[1]†, Annette M. N. Ferguson,[1] Scott C. Chapman,[2] Rodrigo A. Ibata,[3]
Mike J. Irwin,[4] Geraint F. Lewis,[5] Alan W. McConnachie[6]

[1]*SUPA, Institute for Astronomy, University of Edinburgh, Royal Observatory, Blackford Hill, Edinburgh EH9 3HJ, UK*
[2] *Department of Physics and Atmospheric Science, Dalhousie University, Coburg Road, Halifax B3H1A6, Canada*
[3] *Observatoire de Strasbourg, 11, Rue de l'Université, F-67000 Strasbourg, France*
[4] *Institute of Astronomy, Madingley Road, Cambridge CB3 0HA, UK*
[5] *Sydney Institute for Astronomy, School of Physics, A28, University of Sydney, NSW 2006, Australia*
[6] *NRC Herzberg Institute of Astrophysics, 5071 West Saanich Road, Victoria, BC, V9E 2E7, Canada*

ABSTRACT

We present deep *Hubble Space Telescope* Advanced Camera for Surveys observations of the stellar populations in two fields lying at 20 and 23 kpc from the centre of M31 along the south-west semi-major axis. These data enable the construction of colour-magnitude diagrams reaching the oldest main-sequence turn-offs (∼13 Gyr) which, when combined with another field at 25 kpc from our previous work, we use to derive the first precision constraints on the spatially-resolved star formation history of the M31 disc. The star formation rates exhibit temporal as well as field-to-field variations, but are generally always within a factor of two of their time average. There is no evidence of inside-out growth over the radial range probed. We find a median age of ∼7.5 Gyr, indicating that roughly half of the stellar mass in the M31 outer disc was formed before z ∼ 1. We also find that the age–metallicity relations (AMRs) are smoothly increasing from [Fe/H]≃-0.4 to solar metallicity between 10 and 3 Gyr ago, contrary to the flat AMR of the Milky Way disc at a similar number of scale lengths. Our findings provide insight on the roles of stellar feedback and radial migration in the formation and evolution of large disc galaxies.

Key words: galaxies: individual: M31 – Local Group – galaxies: formation – galaxies: evolution – galaxies: structure – galaxies: stellar content

1 INTRODUCTION

Disc galaxies account for a sizeable fraction of the stellar mass in the Universe, yet the details of their formation and evolution are still greatly debated. While much progress has been made in simulating realistic disc galaxies within a cosmological framework (e.g. Aumer et al. 2013; Marinacci, Pakmor, & Springel 2014), many issues remain unresolved. Strong stellar feedback at early epochs is often included in hydrodynamical simulations in order to suppress high redshift star formation, postponing the formation of extended discs until relatively recent times (z≲1 or ∼8 Gyr) when the bulk of the merging is over (e.g. Stinson et al. 2013). This scenario naturally results in the inside-out growth of discs, predicting radial

age gradients and young mean stellar ages at large radii. Direct observations of old and intermediate age stars in outer discs are required to shed light on the efficacy and role of early feedback (e.g. Ferguson & Johnson 2001; Williams et al. 2013).

Once in place, various processes may rearrange the spatial distribution of the stellar populations within galactic discs. For example, it has been shown that stars can undergo large radial excursions within discs due to scattering off transient spirals and other features (e.g. Sellwood & Binney 2002; Minchev et al. 2011). By efficiently mixing stars of different ages and metallicities over kiloparsec scales, this process could lead to a smearing of the star formation history (SFH) and age–metallicity relation (AMR) at a given radius, therefore complicating the interpretation of the resolved fossil record. Determining the importance of this process in real galaxy discs is obviously of paramount importance.

To explore these issues, we have obtained deep *Hubble Space Telescope (HST)* pointings with the Advanced Camera for Surveys (ACS) in order to derive the detailed SFH and AMR at several locations in the outskirts of M31. The SFHs that we calculated for the first 14 fields revealed a global burst of star formation in the
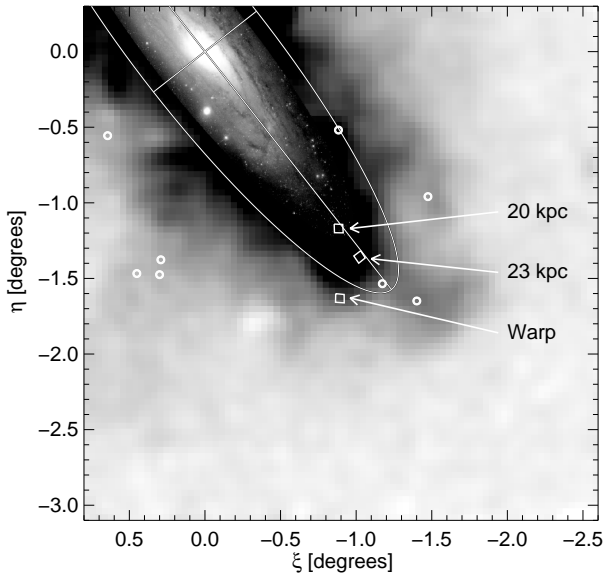
Figure 1. Location of our *HST/ACS* pointings superimposed onto the INT/WFC map of M31's inner halo (Irwin et al. 2005), showing the distribution of evolved giant stars around M31. The three fields analyzed in this work are shown as open squares, while the open circles represent some of the fields studied in Papers I and II. The ellipse has a semimajor axis of 2° (27 kpc) and represents an inclined disc with $i = 77°.5$ and position angle of 38°.1.

M31 outer disc roughly 2 Gyr ago, and allowed us to determine the nature and origin of the various substructures in the outer disc and inner halo (Bernard et al. 2012, 2015, hereinafter Papers I and II, respectively). In this Letter, we present the SFHs calculated for three very deep fields located between 20 and 25 kpc from the centre of M31 along the south-west semi-major axis. Based on colour-magnitude diagrams (CMDs) that reach back to the oldest main-sequence turn-offs (MSTO), these data provide the first precision view of the spatially-resolved SFH in *any* disc galaxy and lead to a number of interesting conclusions about the assembly history of the M31 outer disc. The paper is structured as follows: in Section 2, we present the observations and the data reduction steps, while the CMD-fitting method is briefly described in Section 3. The resulting SFHs and our interpretation of the results are discussed in Section 4.

2   OBSERVATIONS AND DATA REDUCTION

The 20 and 23 kpc fields were observed with the ACS onboard the *HST* (proposal GO-13018, P.I.: A. Ferguson) between 2013 May and August. As the goal of the observations was to study the history of the outer thin disc, the fields were placed very close to the semi-major axis. When combined with the *Warp* field[1] analysed in Paper I, the three fields probe a range of galactocentric distance from 20.1 to 25.4 kpc along the southwest thin disc, corresponding to ~3.8 to 4.8 scalelengths in the M31 disc assuming

$R_d = 5.3 \pm 0.5$ kpc (Courteau et al. 2011). In terms of radial scalelengths, we note that the radius of our innermost field is comparable to that of the solar neighbourhood[2]. Our fields are shown as open squares in Fig. 1, overplotted on a map of the surface density of red giant branch (RGB) stars from the INT/WFC survey of Irwin et al. (2005). The *HST* field lying on the major axis just inside the 27 kpc ellipse is the *Outer Disc* field studied in Paper I, for which we could not calculate the SFH because of strong differential reddening from dust within M31; the other open circles represent some of the inner halo and substructure fields for which SFHs were derived in Paper II. While the *Warp* was observed for 10 *HST* orbits, we obtained 13 orbits per field for each of the new fields in order to compensate for the effect of higher stellar density and background flux. A detailed summary of observations including coordinates, foreground color excess, radial distances, and exposure times is given in Table 1.

The photometry and artificial star tests were carried out following identical methods as those described in Paper I. The only difference here is that we took advantage of the images corrected for the charge transmission inefficiency ('FLC') provided by the *HST* pipeline (e.g. Anderson & Bedin 2010; Ubeda & Anderson 2012). The stellar photometry was carried out on the individual exposures with the standard DAOPHOT/ALLSTAR/ALLFRAME suite of programs (Stetson 1994). They were then cleaned of non-stellar objects by applying cuts on the photometric parameters given by ALLFRAME, namely the photometric uncertainty ($\sigma \leqslant 0.3$) and the sharpness, describing how much broader the profile of the object appears compared to the profile of the PSF ($|\mathrm{SHARP}| \leqslant 0.3$). After cleaning, the CMDs contain 353 918 and 296 731 stars, respectively, compared to 185 335 in the *Warp* with the same quality cuts. The final photometry was calibrated to the VEGAMAG system following the prescriptions of Sirianni et al. (2005) and the revised ACS zeropoints[3], then to absolute magnitude by taking into account the distance to M31 ((m−M)$_0$=24.47; e.g. McConnachie et al. 2005), and the foreground reddening from the Schlegel, Finkbeiner & Davis (1998) extinction maps together with the updated coefficients from Schlafly & Finkbeiner (2011). Note that the CMD-fitting technique used in this paper minimizes the impact of the uncertainties in distance, mean reddening, and photometric zero-points on the solutions by shifting the observed CMD with respect to the artificial CMD; therefore, any small errors in these quantities do not affect the results.

While great care was taken to place the fields in areas of low dust extinction by using the H I maps from Braun et al. (2009), we found that the *23 kpc* field is affected by mild differential reddening due to dust in M31. We used the same method as in Paper I for the *Outer Disc* field to quantify it. We were not able to correct the areas with measureable differential reddening, but found that ~40 percent of the ACS field was not affected. In the following we only use the ~120 000 stars that reside in the unaffected areas.

The resulting CMDs for the two new fields plus the *Warp* are shown in Fig. 2; only 120 000 stars per CMD are shown to ease the comparison. Selected isochrones and a theoretical zero-age horizontal-branch (ZAHB) from the BaSTI library (Pietrinferni et al. 2004) are shown as labeled in the inset, both to indicate the location of the MSTOs and as a guide for comparing

---

[1] This field lies in the southern stellar warp, which bends strongly away from the major axis. As a result, its true radius in the disc could be somewhat larger than its projected radius.

[2] The Sun is located ~3.6 scalelengths from the Galactic centre, assuming $R_{d,MW} \sim 2.2$ kpc (e.g. Bovy & Rix 2013) and $R_0 = 8$ kpc (e.g. Malkin 2013).

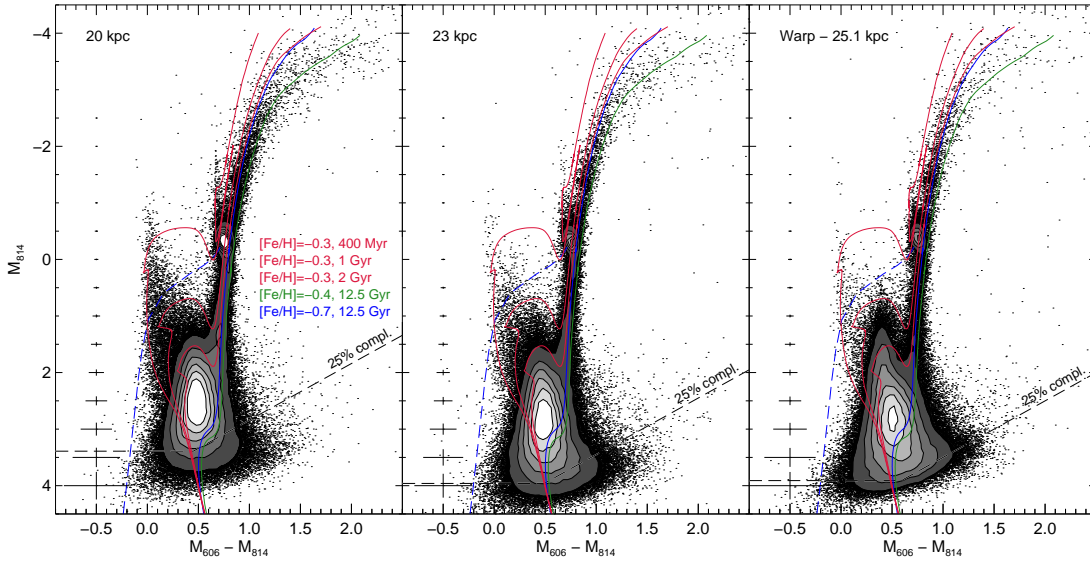[3] http://www.stsci.edu/hst/acs/analysis/zeropoints.

Figure 2. CMDs for the *20 kpc* (left), *23 kpc* (middle), and *Warp* (right) fields, where selected isochrones (solid lines) and a ZAHB (long-dashed line) from the BaSTI library (Pietrinferni et al. 2004) are overlaid and labelled in the inset. Only 120 000 stars per CMD are shown. The error bars show the mean photometric errors as a function of magnitude. The contour levels correspond to $[20, 40, 60, 80, 100, 120] \times 10^3$ stars mag^{-2}. The 25% completeness limit from the artificial stars tests is shown by the dashed lines.

Table 1. Summary of Observations

Field	20 kpc	23 kpc
RA (J2000)	00:38:05.8	00:37:23.8
Decl. (J2000)	+40:05:35	+39:54:00
R^a (kpc)	20.1	23.3
E(B−V)^b	0.053	0.055
Dates	2013 May 28–Jun 2	2013 Jul 31–Aug 10
$t_{F606W}{}^c$ (s)	4×1149+8×1245=14 556	4×1145+8×1240=14 500
$t_{F814W}{}^c$ (s)	4×1149+10×1245=17 046	4×1145+10×1242=17 000

^{a} Galactocentric distance.
^{b} Values from Schlafly & Finkbeiner (2011).
^{c} Individual and total exposure times.

the CMDs. The 25% completeness limit from the artificial star tests is represented as dashed lines. It shows that while the *23 kpc* and *Warp* field have the same photometric depth, the *20 kpc* field is slightly shallower due to the higher stellar density and sky background at the time of the observations. In terms of stellar populations, the main differences between these fields are the gradually less populated main-sequence (at $M_{606} - M_{814} \sim 0$ and $M_{814} \lesssim 2$) with increasing radius, and the RGB of the *Warp* above $M_{814} \sim -1$ being on average bluer by 0.05 mag than in the other fields. The *Warp* also contains a densely populated plume of stars at $M_{606} - M_{814} \sim 0.4$ and $M_{814} \sim 1.5$ that corresponds to a $\sim$2 Gyr old stellar population (see below), and which is not as prominent in the other fields.

3 STAR FORMATION HISTORY CALCULATION

The SFHs were calculated using the technique of synthetic CMD fitting, which provides a detailed and robust quantitative estimate of the star formation rate (SFR) and metallicity ([Fe/H]) at a given time. This involved fitting the observed data with synthetic CMDs to extract the linear combination of simple stellar populations (SSP)

– i.e. each with small ranges of age ($\leqslant$1 Gyr) and metallicity ($<$0.25 dex) – which provides the best fit; the amplitudes of the required SSPs give the rates of star formation as a function of age and metallicity.

The methodology is identical to that used in Papers I and II, although we are now using a new algorithm developed in Python by one of us (EJB). The only notable difference is that the goodness of fit is measured through a Poisson equivalent of χ^2 (see Dolphin 2002) rather than the modified χ^2 statistics of Mighell (1999). Extensive testing has shown that it produces results that are virtually indistinguishible from those obtained with the algorithm used in our previous papers (IAC-POP/MINNIAC; e.g. Hidalgo et al. 2011). This can be verified by comparing the SFH of the *Warp* that was calculated using the new algorithm (see Fig. 3) with Fig. 6 in Paper I. The advantages of the new approach are twofold: the algorithm is at least an order of magnitude faster – a necessary efficiency in view of the ever-increasing size of star catalogues – and it is significantly easier to use. We therefore refer the interested reader to Papers I and II for a detailed description of the assumptions and fitting procedure.

4 RESULTS AND DISCUSSION

The resulting SFHs are presented in Fig. 3, where the top and bottom panels show the evolution of the SFR and of the metallicity, respectively. The redshift scale was constructed assuming the WMAP7 cosmological parameters (Jarosik et al. 2011). In all fields, we find that star formation began early on (z $\gtrsim$ 2) and occurred more or less continuously across the history of the disc. This indicates that M31 was already a large disc galaxy at high redshift and could be a direct descendent of the large disc systems identified in distant redshift studies (e.g. Förster Schreiber et al. 2009; van Dokkum et al. 2013). The SFHs exhibit complex temporal variations; aside from the strong decline over the last 2 Gyr, these variations are not clearly correlated from field to field. Nonetheless, the
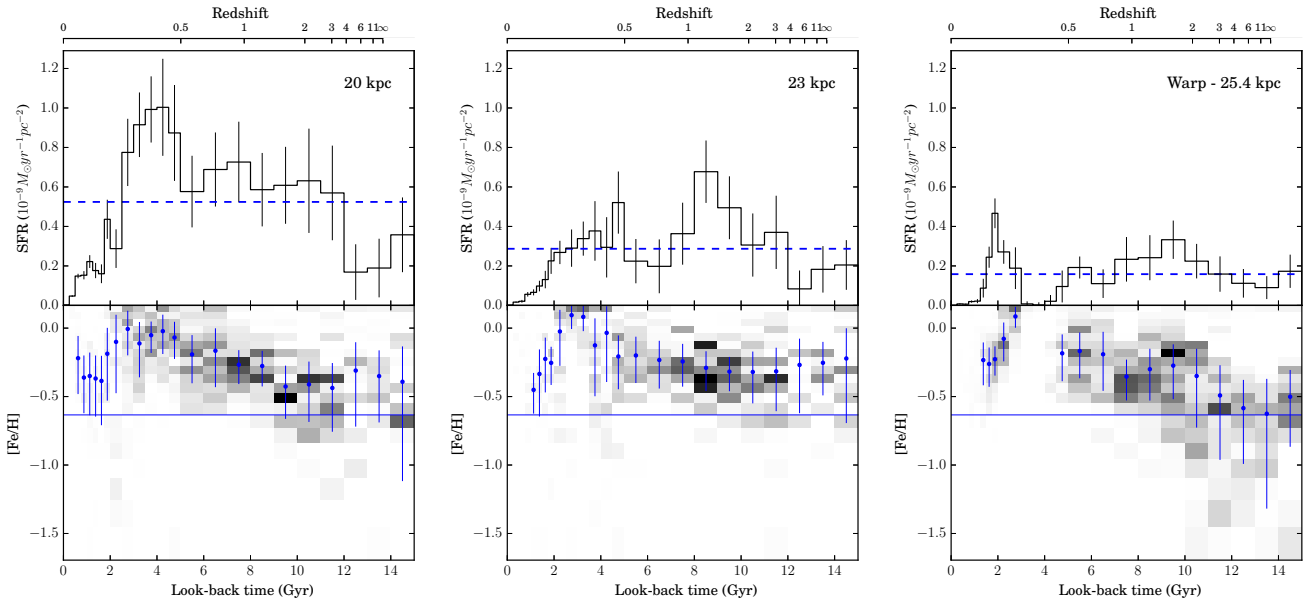
Figure 3. Evolution of the SFR (top) and metallicity (bottom) as a function of time for the three fields, displayed on the same absolute scale. The dashed lines in the top panels show the average SFR over the age of the disc. In the bottom panels, the grayscale is proportional to the stellar mass formed in each bin. The filled circles and error bars show the mean metallicity and standard deviation in the age bins representing at least 1 percent of the total mass of stars formed; the solid blue line serves to guide the eye.

SFR in a given field remains within a factor of ~ 2 of its time average, indicating that very strong bursts of star formation have not dominated the mass build-up in the stellar disc. As expected from the decreasing stellar density with increasing galactocentric radius, the average SFR decreases by a factor ~ 3.3 over the radial range spanned by our data (roughly one scalelength).

A particular feature that stands out in the SFH of the *Warp* is the burst of star formation ~ 2 Gyr ago, associated with the onset of a decrease in global metallicity, that we first detected in Paper I and later found to be widespread in more distant (R $\gtrsim 25$ kpc) fields in M31 (Paper II). Interestingly, while the decrease in [Fe/H] is clearly measured in the two new fields presented here, we do not detect any clear enhancement in the SFR at that epoch. The 20 kpc field does show an enhanced period of star formation activity but this is not as pronounced as the *Warp* burst, and occurs at earlier epochs (3-5 Gyr), so it is not clearly related. We thus conclude that either the 2 Gyr burst was confined to the very outer disc, or that it had much greater significance there. These findings appear to be at odds with SFHs calculated by Williams et al. (2015) in the northern inner disc of M31, which show a ubiquitous strong burst 2-4 Gyr ago in fields ranging from 3–20 kpc. The reason for this discrepancy is presently not clear, although we note that their result is largely based on modelling evolved stars (red clump and RGB) as age indicators, which is not as robust as modelling the main sequence turn-offs in our much deeper data.

To facilitate comparison, Fig. 4 combines the SFHs of our three fields, where the top and bottom panels show respectively the cumulative mass fraction and the AMR as a function of time. The top panel reaffirms that even though the details of the stellar mass growth vary between the fields, all three show significant star formation at $z \gtrsim 1$. Combining all three fields, the median stellar age in the outer disc fields is ~ 7.5 Gyr. To test the reliability of these old ages, we ran constrained SFH calculations where only model populations younger than a given age (8 Gyr, 10 Gyr) were

allowed. While this affected the ability of the algorithm to fit the observed CMD, the median age of the populations did not change. With the caveat that our fields span only one scalelength in radius, there is no signal of inside-out growth in our data. The epoch at which 50% of the present-day stellar mass was in place is 6.9, 8.2, and 8.6 Gyr for the 20 kpc, 23 kpc, and *Warp* fields, respectively. The mild trend of older mean age for increasing radius in M31 is in contrast to some recent integrated light analyses of local galaxies (e.g. Pérez et al. 2013).

The bottom panel of Fig. 4 shows that, for the past 9-10 Gyr, the AMRs of the three fields are very similar within the uncertainties. All start from a moderate level of pre-enrichment and all exhibit a clear decline in the last 3 Gyr. However, we find that the older populations of the *Warp* are considerably more metal-poor than in the 20 and 23 kpc fields, consistent with the slightly bluer RGB in that field (see Fig. 2). This variation is in keeping with the mild abundance gradient that has been measured in this part of the M31 disc (e.g. Kwitter et al. 2012).

However, the most striking feature of these AMRs is the relatively tight, smoothly increasing metallicity between ~ 10 and 3 Gyr ago. This is in stark contrast with the flat AMR of the solar neighbourhood over the same age range (e.g. Haywood 2008; Casagrande et al. 2011). This comparison is relevant since our 20 kpc field in M31 is located at roughly the same number of radial scalelengths as the Sun in the Milky Way. We compare the Geneva-Copenhagen Survey (GCS; Casagrande et al. 2011) AMR[4] with ours in the bottom panel of Fig. 4; it shows that their analysis revealed no metallicity increase in the past 10 Gyr, compared to the enhancement of about 0.4 dex that we have measured in the disc of M31. We note that more recent works on the AMR of the solar neighbourhood based on high resolution spectra (Haywood et al.

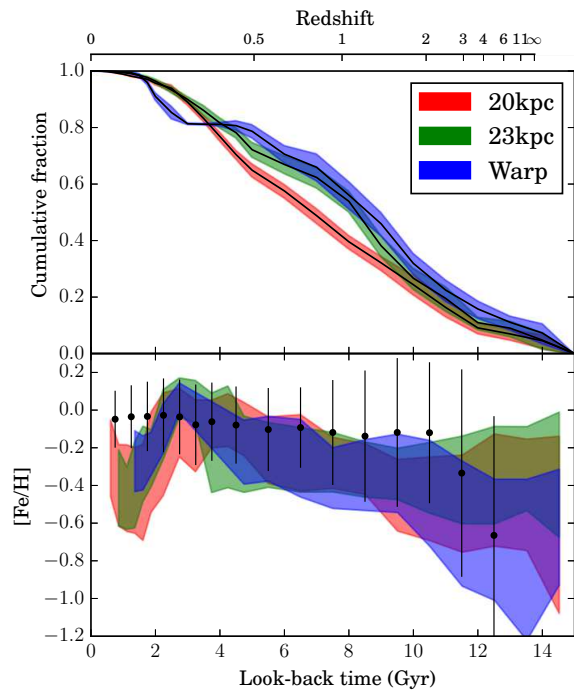[4] Where the age is their "BaSTI Max likelihood age".

Figure 4. Comparison of the SFHs of the three fields, showing the evolution of the cumulative mass fraction (top) and metallicity (bottom), as labeled in the inset. The integrated stellar mass density in each field at the present-day is 3.9, 2.1 and $1.2 \times 10^6 \mathrm{M}_\odot \, \mathrm{kpc}^{-2}$ for the 20 kpc, 23 kpc, and *Warp* fields, respectively. In the bottom panel, the contours correspond to the 1-σ envelope for the age bins representing at least 1 percent of the total mass of stars formed, shown as blue error bars in Fig. 3. The black filled circles with error bars show the AMR of the solar neighbourhood (mean metallicity and standard deviation) from a reanalysis of the Geneva-Copenhagen Survey (Casagrande et al. 2011) for comparison.

2013; Bergemann et al. 2014) do find a clear metallicity increase before about 8 Gyr ago, but a similarly flat AMR since $z \sim 1$.

The difference between the AMRs of the M31 and the Milky Way discs may indicate different formation and/or subsequent evolution histories. The flattening and high dispersion of the AMR in the solar neighbourhood is often ascribed to effects of radial migration in the disc due to non-axisymmetric perturbations of the gravitational potential (e.g. Sellwood & Binney 2002), this region containing stars born in a wide range of galactocentric distances. The increasing AMR in the outer disc of M31, as well as the complex and differing SFH behaviours observed in the three fields, suggests that migration in this galaxy, or at least this part of the galaxy, has been less efficient than in the solar neighbourhood. For example, it is likely that the old, most metal-poor component of the *Warp* would have had sufficient time to contaminate the *23 kpc* field had migration been significant. The different migration efficiencies may be related to the different dynamical properties of the M31 and Milky Way discs: Vera-Ciro et al. (2014) have shown that the efficiency of radial migration is a strong function of the vertical velocity dispersion, the stars spending more time near the disc plane being more affected by the non-axisymmetric perturbations. The measurements of Dorman et al. (2015) in the disc of M31 indicate a velocity dispersion at a given age that is more than twice as large as in the Milky Way (see also Collins et al. (2011)), potentially providing an explanation for the lack of migration. The old age of the M31 outer disc provides further indirect support for this

idea, since disc galaxies observed at $z \sim 2$ are often highly turbulent (e.g. Förster Schreiber et al. 2009).

In summary, our analysis of deep CMDs that reach back to the oldest MSTOs have enabled the first precision constraints on the radial variation of the star formation history in the M31 outer disc. Roughly half of the stellar mass in our fields was formed before $z \sim 1$, indicating that the extended M31 disc was in place and actively forming stars at high redshift. Stellar feedback was not strong enough to significantly delay the formation of the outer disc. Our results also suggest radial migration has not played a major role in rearranging the stellar populations at large radii in M31. Notably, a well-defined AMR is seen in all fields, in marked contrast the flat AMR seen in the Milky Way at similar galactocentric distances. Our findings provide new insight on processes relevant for modelling the evolution of disc galaxies, issues which we will explore in more detail in future work.

REFERENCES

Anderson J., Bedin L. R., 2010, PASP, 122, 1035
Aumer M., White S. D. M., Naab T., Scannapieco C., 2013, MNRAS, 434, 3142
Bergemann M., et al., 2014, A&A, 565, AA89
Bernard E. J., et al., 2012, MNRAS, 420, 2625
Bernard E. J., et al., 2015, MNRAS, 446, 2789
Bovy J., Rix H.-W., 2013, ApJ, 779, 115
Braun R., Thilker D. A., Walterbos R. A. M., Corbelli E., 2009, ApJ, 695, 937
Casagrande L., Schönrich R., Asplund M., Cassisi S., Ramírez I., Meléndez J., Bensby T., Feltzing S., 2011, A&A, 530, AA138
Collins M. L. M., et al., 2011, MNRAS, 413, 1548
Courteau S., Widrow L. M., McDonald M., Guhathakurta P., Gilbert K. M., Zhu Y., Beaton R. L., Majewski S. R., 2011, ApJ, 739, 20
Dolphin A. E., 2002, MNRAS, 332, 91
Dorman C. E., et al., 2015, ApJ, 803, 24
Ferguson A. M. N., Johnson R. A., 2001, ApJL, 559, L13
Förster Schreiber N. M., et al., 2009, ApJ, 706, 1364
Haywood M., 2008, MNRAS, 388, 1175
Haywood M., Di Matteo P., Lehnert M. D., Katz D., Gómez A., 2013, A&A, 560, AA109
Hidalgo S. L., et al., 2011, ApJ, 730, 14
Irwin M. J., Ferguson A. M. N., Ibata R. A., Lewis G. F., Tanvir N. R., 2005, ApJL, 628, L105
Jarosik N., et al., 2011, ApJS, 192, 14
Kroupa P., 2002, Sci, 295, 82
Kwitter K. B., Lehman E. M. M., Balick B., Henry R. B. C., 2012, ApJ, 753, 12
Marinacci F., Pakmor R., Springel V., 2014, MNRAS, 437, 1750
Malkin Z. M., 2013, Astron. Rep., 57, 128
McConnachie A. W., Irwin M. J., Ferguson A. M. N., Ibata R. A., Lewis G. F., Tanvir N., 2005, MNRAS, 356, 979
Mighell K. J., 1999, ApJ, 518, 380
Minchev I., Famaey B., Combes F., Di Matteo P., Mouhcine M., Wozniak H., 2011, A&A, 527, AA147
Pérez E., et al., 2013, ApJ, 764, L1
Pietrinferni A., Cassisi S., Salaris M., Castelli F., 2004, ApJ, 612, 168
Schlafly E. F., Finkbeiner D. P., 2011, ApJ, 737, 103
Schlegel D. J., Finkbeiner D. P., Davis M., 1998, ApJ, 500, 525
Sellwood J. A., Binney J. J., 2002, MNRAS, 336, 785
Sirianni M., et al., 2005, PASP, 117, 1049

Stetson P. B., 1994, PASP, 106, 250

Stinson, G. S., Brook, C., Macciò, A. V., et al. 2013, MNRAS, 428, 129

Tokovinin A., 2014, AJ, 147, 87

Ubeda L., Anderson J., 2012, acs..rept, 3

van Dokkum P. G., et al., 2013, ApJ, 771, L35

Vera-Ciro C., D'Onghia E., Navarro J., Abadi M., 2014, ApJ, 794, 173

Williams B. F., Dalcanton J. J., Stilp A., Dolphin A., Skillman E. D., Radburn-Smith D., 2013, ApJ, 765, 120

Williams B. F., et al., 2015, ApJ, 806, 48